Assessment of design mechanical parameters and partial safety factors for Wire-and-Arc Additive Manufactured stainless steel

Laghi, Vittoria; Palermo, Michele; Gasparini, Giada; Veljkovic, Milan; Trombetti, Tomaso

DOI
10.1016/j.engstruct.2020.111314

Publication date
2020

Document Version
Final published version

Published in
Engineering Structures

Citation (APA)
Laghi, V., Palermo, M., Gasparini, G., Veljkovic, M., & Trombetti, T. (2020). Assessment of design mechanical parameters and partial safety factors for Wire-and-Arc Additive Manufactured stainless steel. *Engineering Structures*, *225*, Article 111314. https://doi.org/10.1016/j.engstruct.2020.111314

Engineering Structures 225 (2020) 111314

Contents lists available at ScienceDirect

Engineering Structures

journal homepage: www.elsevier.com/locate/engstruct

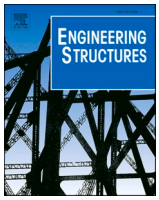

Assessment of design mechanical parameters and partial safety factors for Wire-and-Arc Additive Manufactured stainless steel

Vittoria Laghi [a,*], Michele Palermo [a], Giada Gasparini [a], Milan Veljkovic [b], Tomaso Trombetti [a]

[a] Department of Civil, Chemical, Environmental and Materials Engineering – University of Bologna, Viale del Risorgimento, 2, 40136 Bologna, Italy
[b] Faculty of Civil Engineering and Geosciences – University of Technology Delft, Stevinweg, 1, 2628CN Delft, the Netherlands

ARTICLE INFO

Keywords:
Additive manufacturing
Wire-and-arc
Stainless steel structures
Calibration from experiments
Eurocode 0
Partial factors

ABSTRACT

Early investigations suggest that the use of Additive Manufacturing (AM) technologies for construction has the potential to decrease labor costs, reduce material waste, and create customized complex geometries that are difficult to be manufactured using conventional construction techniques. Nevertheless, the full exploitation of AM technologies requires data on the material mechanical properties so that reliable and safety design requirements can be developed. Among different metal AM techniques, the so-called Wire-and-Arc Additive Manufacturing (WAAM) results to be potentially suitable to realize large-scale structural elements of any shape and size. However, the results of early experimental tests on WAAM-produced alloys suggest the need of ad-hoc considerations to properly interpret the geometrical and mechanical features of the printed outcomes.

The present study analyzes the data obtained from the experimental results of tensile tests carried out on WAAM-produced 308LSi stainless steel elements with the purpose of calibrating design values and partial safety factors. In order to account for the anisotropic behavior proper of WAAM-produced elements, the design values of the main mechanical parameters have been calibrated for the three main orientations of the specimens with respect to the deposition layer. The calibrated design values and partial safety factors for the yielding and ultimate tensile strength are compared with recommended values for stainless steel structures as provided by EN1993:1-4 - Eurocode 3 (EC3). Additional considerations upon the Young's modulus values, highly influenced by the anisotropic behavior of WAAM-produced stainless steel, are presented as well.

1. Introduction

Automation in construction industry has recently grown thanks to the diffusion of digital fabrication processes which nowadays are currently employed in other industries such as aerospace and automotive [1–4]. Recent developments of Additive Manufacturing (AM) process in construction have seen the application of 3D printing techniques to realize a new generation of structures in concrete, polymers and metals [5]. In applications for steel structures, Powder-Based Fusion (PBF) technology has been adopted to realize ad-hoc connections parametrically designed either for structural optimization purposes [6] or to create free-form gridshells [7]. However, due to the intrinsic geometrical constraints of the printer environment (enclosed in a box of typically 250-mm side), the application of PBF process is limited to the realization of small-size connections and structural details [8].

In order to realize real-scale structural elements without ideally any geometrical constraints either in size or shape, the most suitable manufacturing solution for metallic elements is the so-called Wire-and-Arc Additive Manufacturing (WAAM) process. This 3D printing technology uses off-the-shelf traditional welding equipment mounted on top of either numerically-controlled robotic arms or cartesian machines, able to realize large-scale elements. The first proof-of-concept of the possibilities of the WAAM process in construction is represented by the MX3D Bridge project [9], whose outcome is the first 3D-printed stainless steel footbridge completed in 2018 which will be placed in Amsterdam city center by 2020 (Fig. 1). The main advantage presented by WAAM process relies on the possibility to create new shapes and forms following the breakthrough design tools for modern architecture as algorithm-aided design with in principle no constraints either in shape or size of the printed outcome. At the same time, the WAAM process ensures fast production with good quality outcome both in terms of geometrical precision and mechanical properties. On the other hand, two additional considerations must be addressed when dealing with WAAM-produced elements. First, the inherent surface roughness proper of WAAM process could influence the mechanical response. Moreover,

* Corresponding author.
E-mail address: vittoria.laghi2@unibo.it (V. Laghi).

https://doi.org/10.1016/j.engstruct.2020.111314
Received 17 December 2019; Received in revised form 1 June 2020; Accepted 9 September 2020
Available online 14 October 2020

Nomenclature

The following symbols are used in this paper:

E	Young's modulus
$E_{0.1\%}$	value of Young's modulus corresponding to 0.1%-fractile from the best-fit Log-normal distribution
$E_{5\%}$	value of Young's modulus corresponding to 5%-fractile from the best-fit Log-normal distribution
$E_{50\%}$	value of Young's modulus corresponding to 50%-fractile from the best-fit Log-normal distribution
$E_{95\%}$	value of Young's modulus corresponding to 95%-fractile from the best-fit Log-normal distribution
$E_{99.9\%}$	value of Young's modulus corresponding to 99.9%-fractile from the best-fit Log-normal distribution
KS	Kolmogorov-Smirnov test for best-fit statistical distributions
V_{exp}	standard deviation of the experimental statistical distribution
V_L	standard deviation of the best-fit Log-normal distribution
V_N	standard deviation of the best-fit Normal distribution
V_W	standard deviation of the best-fit Weibull distribution
V_X	standard deviation of the generic variable X
X	population (experimental values) of the generic mechanical parameter
X_d	design value of the generic variable (according to EC0 [36])
X_k	characteristic value of the generic variable (according to EC0 [36])
f_t	ultimate tensile strength
$f_{t,0.1\%}$	value of ultimate tensile strength corresponding to 0.1%-fractile from the best-fit Log-normal distribution
$f_{t,5\%}$	value of ultimate tensile strength corresponding to 5%-fractile from the best-fit Log-normal distribution
f_{td}	design value of ultimate tensile strength
f_{tk}	characteristic value of ultimate tensile strength
f_y	yielding stress
$f_{y,0.1\%}$	value of yielding stress corresponding to 0.1%-fractile from the best-fit Log-normal distribution
$f_{y,5\%}$	value of yielding stress corresponding to 5%-fractile from the best-fit Log-normal distribution
f_{yd}	design value of yielding stress
f_{yk}	characteristic value of yielding stress
k_n	calibration coefficient to estimate characteristic values of strength from experiments (according to Annex D of EC0 [36])
m_y	estimation of the mean value of the Log-normal distribution associated to X
s_y	estimation of the standard deviation of the Log-normal distribution associated to X
γ_m	partial safety factor related to each single material property
γ_{m1}	partial safety factor calibrated for the yielding stress
γ_{m2}	partial safety factor calibrated for the ultimate tensile strength
γ_{M0}	partial safety factor for yielding (according to EC0 [36])
γ_{M2}	partial safety factor for fracture (according to EC0 [36])
α_R	FORM sensitivity factor
β	reliability index
μ_{exp}	mean value of the experimental statistical distribution
μ_L	mean value of the best-fit Log-normal distribution
μ_L	mean value of the best-fit Normal distribution
μ_W	mean value of the best-fit Weibull distribution
σ_{exp}	standard deviation of the experimental statistical distribution
σ_L	standard deviation of the best-fit Log-normal distribution
σ_N	standard deviation of the best-fit Normal distribution
σ_W	standard deviation of the best-fit Weibull distribution

the marked anisotropy also evidenced from the material microstructure is to take into account when defining the main mechanical parameters. Different process parameters result in different surface finishing and microstructure, both affecting the mechanical response [10].

In this regard, while several research effort has been made to study the mechanical and microstructural behavior of PBF-produced alloys [8,11–14], current research on WAAM-produced alloys focuses mainly on the microstructural analysis with limited information on either mechanical parameters or the anisotropic behavior [15–19]. Indeed, proper mechanical characterization of WAAM steel in terms of the key material properties for structural design (i.e. yielding stress, ultimate tensile strength, Young's modulus and elongation at rupture) and anisotropy is

Fig. 1. The MX3D Bridge [9].

still limited to few studies [20–22]. In the work done by Gordon and co-authors [21], Young's modulus values are reported, indicating values around 130 to 140 GPa, significantly lower than the one registered by the conventional wrought material (about 200 GPa). Haden et al. [20] registered non-negligible anisotropy for WAAM stainless steel specimens in terms of ultimate tensile strength and elongation at rupture. Kyvelou et al. [22] performed tensile tests on WAAM stainless steel specimens along three directions (longitudinal, transversal and diagonal with respect to the deposition layers), whose results confirmed marked anisotropy with a wide range of Young's modulus values for the different orientations tested.

Since 2017, the authors have been studying both microstructural and mechanical characterization of WAAM-produced stainless steel elements for structural engineering applications [23–25] as academic partner of the MX3D Bridge project.

A first overview of the geometrical and mechanical characterization of WAAM elements for structural engineering applications is presented in [23,24]. From that, a more detailed study on the material properties of WAAM 308LSi stainless steel from the mechanical and metallurgic point of view is presented in [25].

The present work analyzes the data obtained from the mechanical tests with the purpose of providing a first calibration of the design mechanical properties and partial safety factors of WAAM-produced 308LSi stainless steel elements for structural purposes.

2. The Wire-and-Arc Additive Manufacturing process

A basic AM system consists of a combination of a motion system, heat source and feedstock [26]. In particular, the combination of an electric arc as heat source and wire as feedstock is referred to as Wire-and-Arc Additive Manufacturing (WAAM), which currently uses standard off-the-shelf welding equipment, such as welding power source, torches and wire feeding system, while motion is provided by either robotic systems, computer numerical-controlled gantries or cartesian machines. WAAM's layer height is commonly in the range of 1 to 2 mm, resulting in an expected surface roughness of about 0.5 mm for single track deposits. As a result, this process is not considered net shape, as machining is required to finish the part, thus being better suited for low- to medium-complexity and medium- to large-scale elements, as those implemented in structural engineering [20,27–29].

When dealing with WAAM-produced structural elements it is necessary to first codify specific issues related to: (i) the set of process parameters; (ii) the wrought material; (iii) the printing strategy. Furthermore, given the novelty of the process especially for structural engineering applications, there is very limited database of experimental results to provide sufficient information for the structural response of WAAM-produced metallic structural elements. The present work focuses on the particular set-up configuration of WAAM process adopted by the Dutch company MX3D [9] to realize the first 3D-printed steel footbridge. MX3D makes use of a Gas Metal Arc Welding (GMAW) process, characterized by a continuous wire electrode which is drawn from a reel by an automatic wire feeder. The wire is fed through the contact tip in the welding torch. The heat is transferred from the welding arc and the internal resistive power causes the wire to melt [30,31]. The motion system consists of industrial multi-axis ABB robots which, theoretically, are able to print from any angle. Two different printing strategies can be used: a so-called *continuous printing*, meaning that the material is deposited in continuous layers, and a so-called *dot-by-dot printing*, meaning that the material is deposited by successive points. The effects of these strategies on the metallurgic characteristics have been analyzed in [32,33].

For such reason, the present work is limited to the study of WAAM-produced 308LSi stainless steel elements realized using continuous printing strategy. The specimens (Fig. 2) were realized by MX3D with a fixed set of process parameters, lying within the ranges as shown in Table 1. The welding source used is Gas Metal Arc Welding (GMAW), with pulse welding arc transfer. No arc correction has been adopted during the printing process. The substrate is a printing plate of 1000 × 1000 × 30 mm, with H-type beams welded as support. No external cooling has been used, apart from the process pauses between layers to allow the material to cool down, until it reaches a temperature below the interpass temperature of 150°.

Fig. 2. Tensile specimens cut from WAAM plates: (a) as-printed and (b) after surface milling.

Table 1
Process parameters for WAAM deposition (Courtesy of MX3D [9]).

Process parameters	Details	Value
Deposition power	Current	100–140 A
	Arc voltage	18–21 V
Speed	Welding speed	15–30 mm/s
	Wire feed rate	4–8 m/min
	Deposit rate	0.5–2 kg/h
Distance and angle	Layer height	0.5–2 mm
	Electrode to layer angle	90°
Wire	Wire grade	ER308LSi
	Wire diameter	1 mm
Shield gas	Shield gas type	98% Ar, 2%CO_2
	Shield gas flow rate	10–20 L/min

3. The experimental results

3.1. Material investigation

First investigations on the material properties of WAAM-produced stainless steel material were conducted in collaboration with the Metallurgic department of University of Bologna to correlate the key material properties with the microstructural features of the printed outcomes. The results were presented in [25].

Detailed inspection of the microstructure evidenced an oriented grain growth on the specimens. Indeed, WAAM process produced grains oriented perpendicular to the deposition layers, as presented in Fig. 3. Such microstructure affects the mechanical response of specimens oriented at different directions with respect to the printing layers, as demonstrated by the tensile results presented in [22,25].

The microstructural investigations did not detect any significant defects or porosity in the specimens tested. Further details are presented in [25].

3.2. Mechanical properties

Since 2017 a wide experimental campaign has been carried out at the Topography and Structural Engineering Lab of the University of Bologna, in order to assess the main geometrical irregularities and mechanical properties of WAAM-produced stainless steel elements.

Experimental tests were performed on both machined and as-built specimens (Fig. 2) to evaluate the possible influence of the surface roughness, inherent in WAAM printing process, on the tensile response [24].

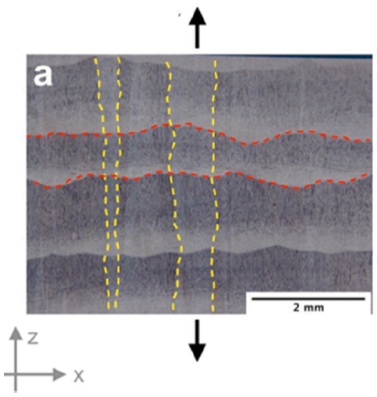

Fig. 3. Microstructural grain growth (yellow) vs. deposition layer (red) for specimens oriented transversally. Black arrows indicate the loading direction. Adapted from [25] (For interpretation of the references to colour in this figure legend, the reader is referred to the web version of this article)

For the purpose of the present work, only tensile test results of machined specimens were considered. In this way, the focus is restricted to the variability of the mechanical properties due to the inherend material behavior only. The effect of the geometrical irregularities proper of the fabrication process will be considered in a further study.

The results are taken from a set of 26 tensile tests performed on samples having different orientations with respect to the deposition layers, as follows: (i) 6 tests on transversal (T) specimens oriented perpendicular to the deposition layers; (ii) 8 tests on longitudinal (L) specimens oriented along the deposition layers; (iii) 12 tests on inclined specimens oriented at 45°, i.e. "diagonal" (D) with respect to the deposition layers (Fig. 4a). For the sake of conciseness, the three different orientations of the specimens with respect to the deposition layers will be hereafter referred to as direction T, L and D. The specimens, extracted along the three main directions as shown in Fig. 4a, were shaped according to ISO 6892–1 [34] (Fig. 4b).

They were previously polished by means of mechanical milling, reducing the final thickness to an average value of 2.5 to 3 mm, starting from the nominal 4-mm thickness of the plates.

Fig. 5 provides an overview of the experimental results by comparing the mean values and standard deviations of the key material properties (0.2% proof stress, ultimate tensile strength, Young's modulus and elongation at rupture) along the three directions. Additional reference values of the key material properties for traditionally-manufactured 304L stainless steel (according to EN1993:1-4 - Eurocode 3 (EC3) [35]) are included as well. It should be noted that Eurocode 3 does not provide reference values for elongation at rupture of 304L stainless steel. The results are also reported in Table 2 in terms of mean values (μ_{exp}), standard deviations (σ_{exp}) and coefficients of variation (V_{exp}).

The results of the experimental tests on WAAM 308LSi stainless steel clearly show an anisotropic behavior of the material, highly influenced by the orientation of the specimens with respect to the deposition layers (directions T, L and D). The mean values of 0.2% proof stress and ultimate tensile strength are similar for specimens oriented along T and L directions, while they increase of about 20% for 0.2% proof stress and 20% for ultimate tensile strength along D direction. Also the coefficients of variation tend to increase for specimens along D direction. The Young's modulus shows the highest sensitivity with respect to the specimens orientation. In particular, the mean value along L direction

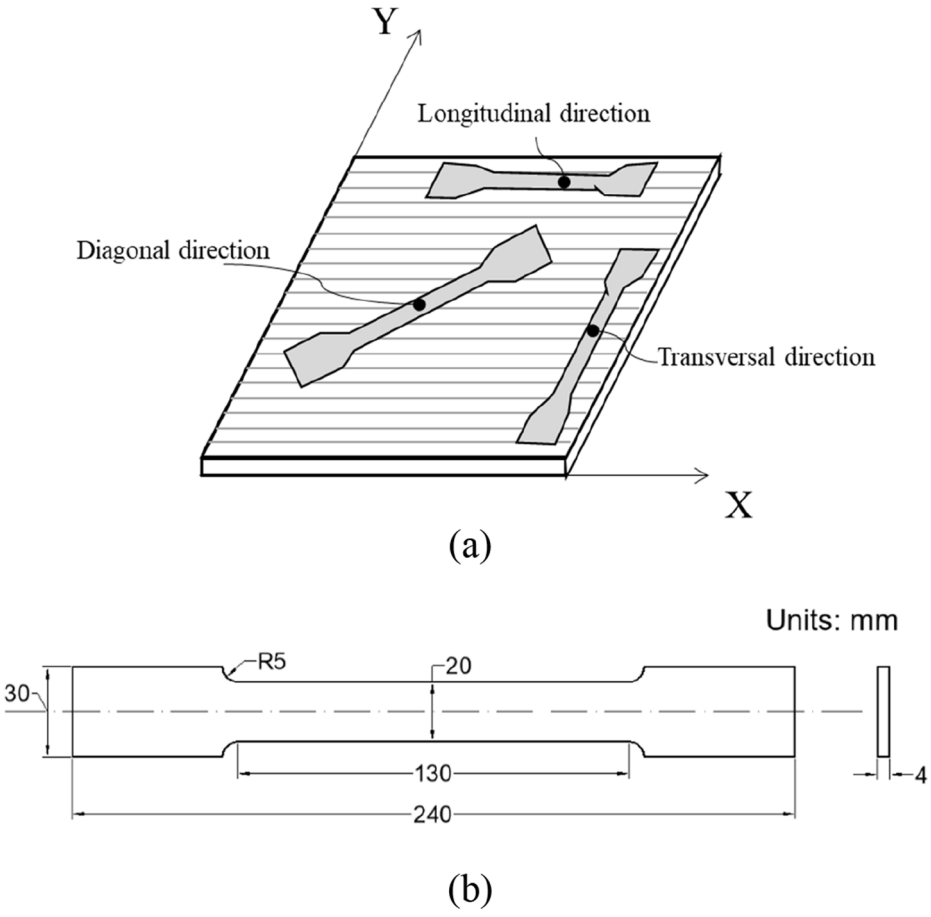

Fig. 4. (a) Orientation of the "dog-bone" shaped specimens cut from plates with respect to the deposition layer (grey lines); (b) geometry and dimensions (mm) of the flat tensile specimens according to ISO 6892–1 [34].

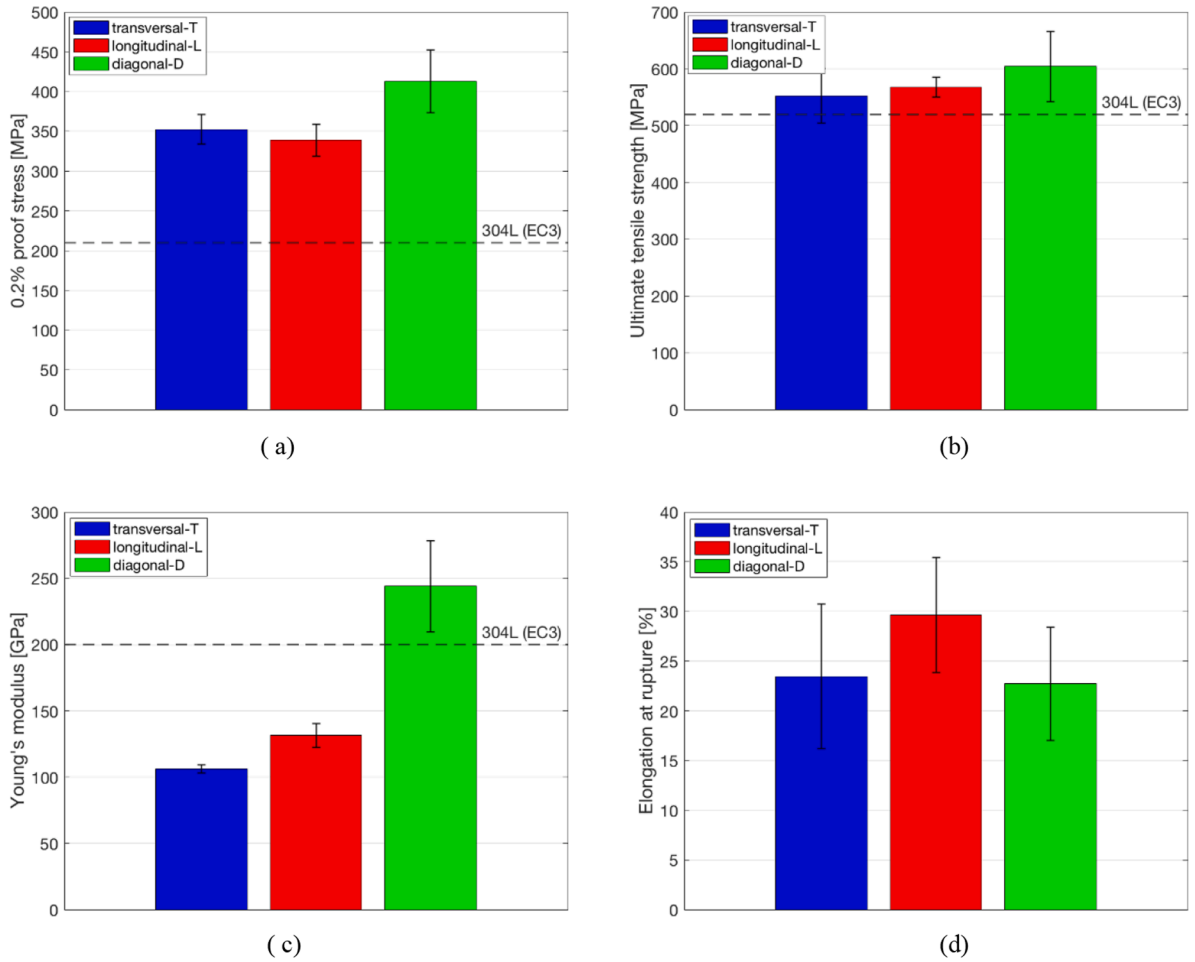

Fig. 5. Key mechanical parameters from the experimental results on WAAM 308LSi stainless steel: (a) 0.2% proof stress; (b) ultimate tensile strength; (c) Young's modulus; (d) elongation at rupture.

Table 2
Key mechanical parameters from the experimental results on WAAM 308LSi stainless steel.

		μ_{exp}	σ_{exp}	V_{exp}
0.2% proof stress [MPa]	T	352.54	18.36	0.052
	L	338.94	20.05	0.059
	D	412.71	39.30	0.095
Ultimate tensile strength [MPa]	T	552.53	48.30	0.087
	L	567.44	17.20	0.030
	D	604.04	61.73	0.102
Young's modulus [MPa]	T	106.09	2.98	0.028
	L	135.51	9.04	0.069
	D	244.00	34.41	0.141
Elongation at rupture [%]	T	23.47	7.27	0.310
	L	29.66	5.78	0.195
	D	22.72	5.70	0.251

increases of about 30% with respect to that along T direction, while the mean value along D direction increases of about 120% with respect to that along T direction. Also the coefficient of variation tends to increase for specimens oriented along D direction. The values of elongation are rupture are, on average, not significantly influenced by the orientation, even though they exhibit a quite large variability due to the influence of the microstructure on the rupture [25]. It is important to notice that Young's modulus values obtained along T and L directions are almost 40% less than the standard value of traditionally-manufactured stainless steel elements [35], while those along D direction are around 20% larger than the standard value. This anisotropic behavior is in line with the orientation of micro-grains growing perpendicular to the deposition layers (see Section 3.1), resulting in an orthotropic elastic model of WAAM material [25]. Similar results are also found in [22]. Average values of 0.2% proof stress and ultimate tensile strength do not significantly differ from those of traditionally-manufactured stainless steel. In order to properly assess the values of Young's modulus during the tensile test, different measuring systems were adopted: (i) strain gauges to locally measure the strain of the specimen during the test; (ii) deformometers for a mean measurement of the strain until first yielding occurs; (iii) optical measuring system by means of Digital Image Correlation technique to obtain information on the full field of strain during the entire test.

In light of the considerable anisotropy evidenced by the experimental results, the statistical interpretation and calibration of structural design values of yielding (0.2% proof) stress and ultimate tensile strength have been carried out differentiating the three main orientations of the specimens (T, L and D). Additional considerations on the Young's modulus are also provided.

4. Statistical interpretation of the experimental results

In this section, a statistical analysis is carried out to evaluate the "best-fit" distributions of the experimental results assuming Normal, Weibull and Log-normal distribution models according to the maximum likelihood estimators. Figs. 6, 7 and 8 provide a comparison between "experimental" (e.g. statistical distributions) and best-fit cumulative distribution functions (CDF) and probability density functions (PDF) for yielding (0.2% proof) stress, ultimate tensile strength and Young's

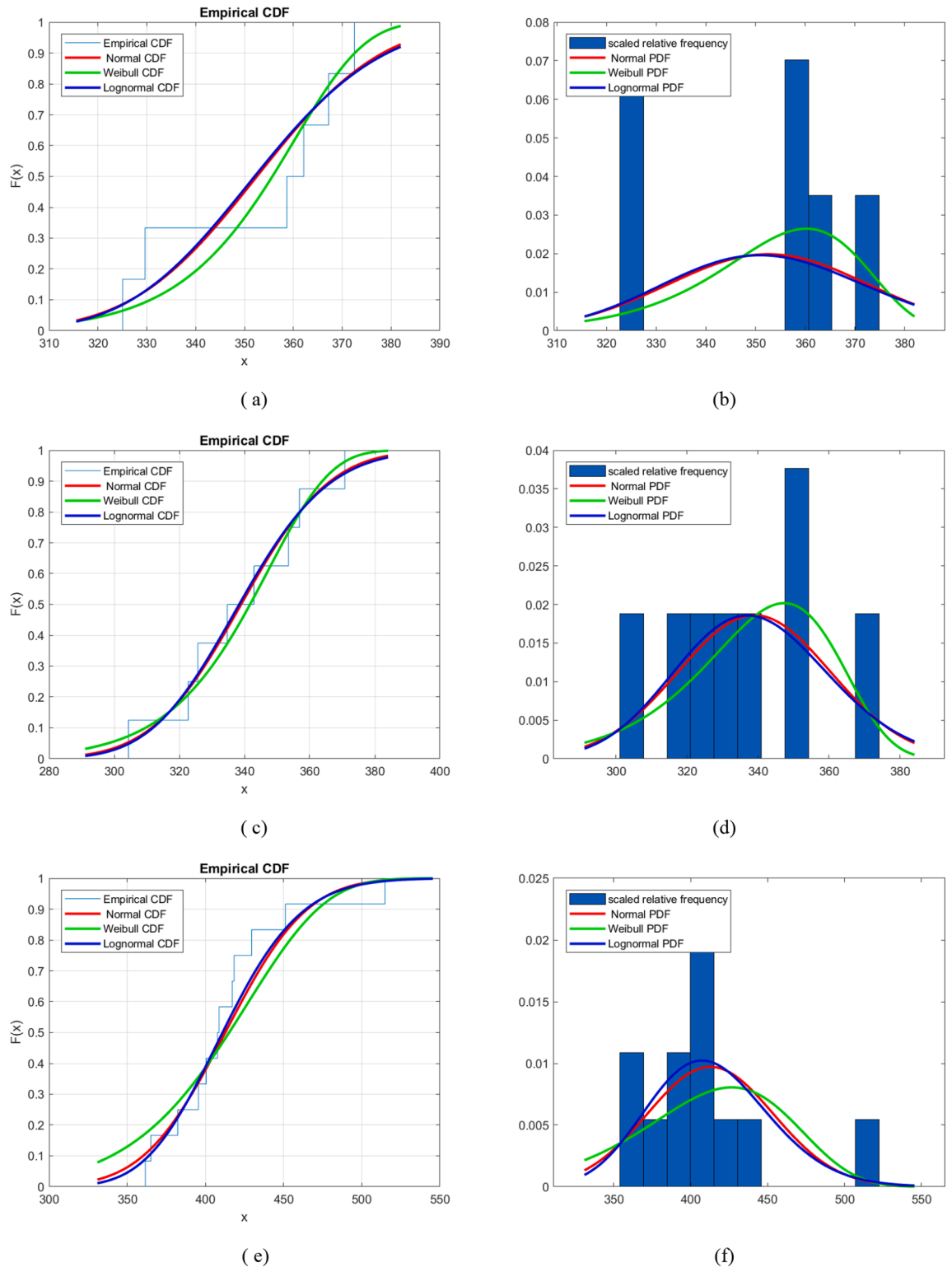

Fig. 6. Statistical distributions of 0.2% proof stress: (a) CDF and (b) PDF for direction T; (c) CDF and (d) PDF for direction L; (e) CDF and (f) PDF for direction D.

modulus, differentiating for the three main orientations of the specimens (T, L and D).

The samples size, although small (from 6 to 12 per direction), is in accordance with the minimum recommended dimension according to Annex C and D of EN1990 - Eurocode 0 (EC0) [36] to perform calibration from experiments, as long as specific values of correction factors (as reported in the provisions) are adopted. The choice of the distribution models was made according to the indications provided in Annex C and D of EC0 for strength data [36].

The mean values and standard deviations of the best-fit distributions are summarized in Table 3. The coefficients of variation for both yielding (0.2% proof) stress and ultimate strength (for all three

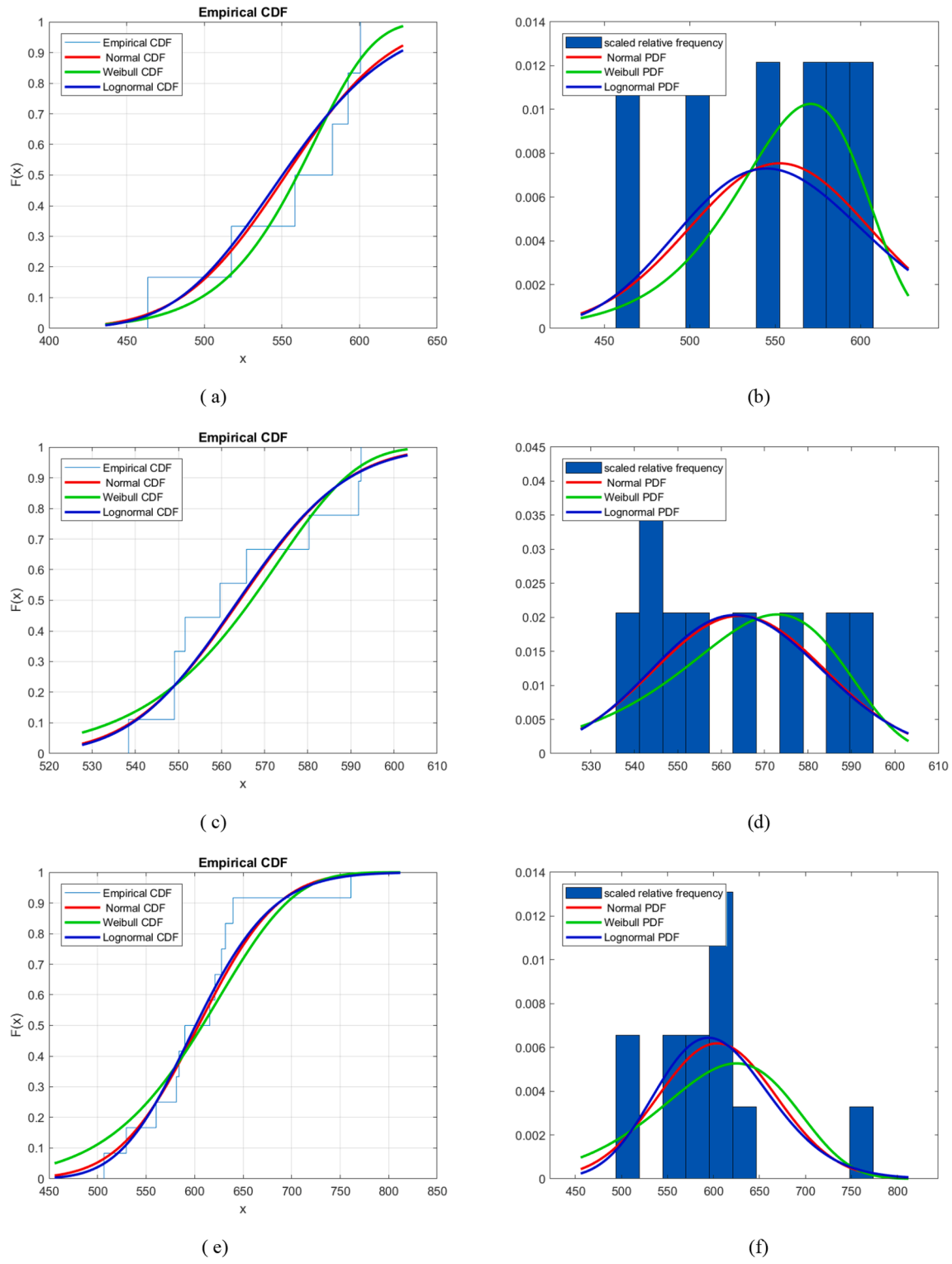

Fig. 7. Statistical distributions of ultimate tensile strength: (a) CDF and (b) PDF for direction T; (c) CDF and (d) PDF for direction L; (e) CDF and (f) PDF for direction D.

distributions along the three directions) are within 2% and 10%, and in line with ranges obtained for traditionally-manufactured steel elements used in construction [37].

Table 4 provides the results of Kolmogorov-Smirnov test in terms of coefficient KS [38] of the best-fit distributions evaluated from maximum likelihood estimators for the experimental data. The obtained KS values range between 0.12 and 0.29. The critical values for $\alpha = 0.05$ are: 0.519 for T specimens, 0.454 for L specimens and 0.375 for D specimens. Overall, the results provide lower values than the critical, thus suggesting that all three distributions provide a good fit with the experimental results. Among the three distributions, the Log-normal distributions provide slightly smaller values of coefficient KS (the average KS value for the Log-normal distributions is around 0.2). Thus, in the next section the Log-normal distributions will be considered to

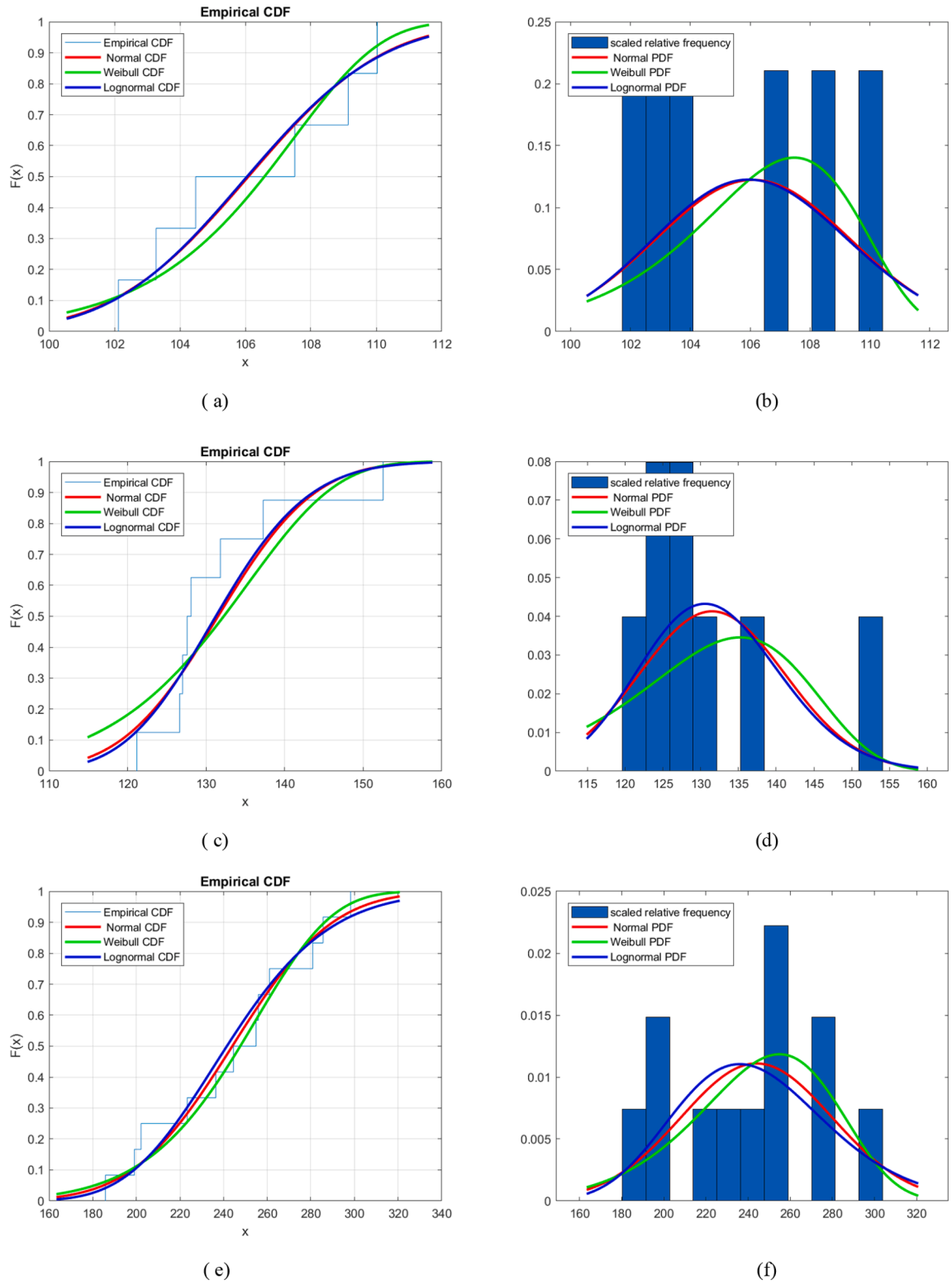

Fig. 8. Statistical distributions of Young's modulus: (a) CDF and (b) PDF for direction T; (c) CDF and (d) PDF for direction L; (e) CDF and (f) PDF for direction D.

calibrate the design values. This is also in accordance with the recommendations provided in EC0 for calibration of design values for strength.

5. Design values of yield and ultimate stress

In this section the attention is paid to the calibration of the design values for the yielding stress (f_{yd}), which corresponds to 0.2% proof stress for stainless steel (according to EC3 [35]), and the ultimate tensile strength (f_{td}).

The calibration of the design values of yielding and ultimate stress and corresponding partial factors is carried out considering two approaches, respectively based on the best-fit distributions (Section 5.1) and on the procedure explained in Annex D of EC0 [36] (Section 5.2).

As far as the Young's modulus is concerned, for traditionally-

Table 3
Mean and standard deviation values of Normal, Log-normal and Weibull best-fit statistical distributions of the mechanical properties of WAAM 308LSi stainless steel.

		NORMAL			WEIBULL			LOGNORMAL		
		μ_N	σ_N	V_N	μ_W	σ_W	V_W	μ_L	σ_L	V_L
0.2% proof stress [MPa]	T	352.54	20.11	0.057	353.24	17.02	0.048	352.65	20.47	0.058
	L	338.94	21.44	0.063	338.69	21.98	0.065	339.04	21.58	0.064
	D	412.71	41.05	0.099	409.59	52.26	0.128	412.83	39.43	0.096
Ultimate tensile strength [MPa]	T	552.53	52.91	0.096	554.49	42.77	0.077	553.07	55.33	0.100
	L	564.22	19.73	0.035	563.64	22.22	0.039	564.25	19.64	0.035
	D	604.04	64.48	0.107	599.66	79.58	0.133	604.24	62.77	0.104
Young's modulus [GPa]	T	106.09	3.26	0.031	106.08	3.26	0.031	106.10	3.26	0.031
	L	131.51	9.66	0.073	130.71	12.49	0.096	131.55	9.29	0.071
	D	244.00	35.95	0.147	244.18	35.12	0.144	244.29	37.17	0.152

Table 4
Kolmogorov-Smirnov test of the Normal, Log-normal and Weibull best fit statistical distributions.

		Kolmogorov-Smirnov test		
		KS_N [–]	KS_W [–]	KS_L [–]
0.2% proof stress	T	0.2863	0.2432	0.2923
	L	0.1265	0.1329	0.1294
	D	0.1951	0.2248	0.1756
Ultimate tensile strength	T	0.2147	0.2265	0.2248
	L	0.1838	0.1934	0.1822
	D	0.2072	0.2512	0.1906
Young's modulus	T	0.1895	0.2360	0.1863
	L	0.2638	0.2639	0.2595
	D	0.1277	0.1285	0.1393

manufactured stainless steel this quantity is commonly considered as deterministic, since its variability is negligible. However, the results of the experimental tests conducted on WAAM-produced stainless steel samples (as shown in Section 3 and in [24,25]) revealed a significant variability in the Young's modulus values, also highly influenced by the orientation of the specimens with respect to the deposition layer. For such reason, considerations upon Young's modulus are presented in a dedicated section (Section 6).

5.1. Calibration based on the best-fit Log-normal distributions

From best-fit Log-normal distributions as evaluated in Section 4, the fractiles corresponding to the characteristic and design values of the key material parameters have been computed. From their ratio, the estimation of the partial factor of safety is evaluated as well.

According to the fundamental principles of reliability analysis as described in EC0 [36], the following fractiles of the random variable associated to the strength parameters are considered:

- 5%-percentile of the distribution, corresponding to the characteristic value;
- 0.1%-percentile of the distribution, corresponding to the design value.

It should be noted that the material partial safety factor for yielding stress ($f_{y,5\%}/f_{y,0.1\%}$) is to be compared with the value of partial factor recommended in EN1993:1–4 [35] for resistance of cross-sections to excessive yielding realized in stainless steel, equal to $\gamma_{M0} = 1.10$. Similarly, the material partial safety factor of the ultimate tensile strength ($f_{t,5\%}/f_{t,0.1\%}$) should be compared to the partial factor recommended in EN1993:1–4 [35] for resistance of cross-sections in tension to fracture realized in stainless steel, equal to $\gamma_{M2} = 1.25$.

5.2. Calibration according to Eurocode 0

EC0 [36] gives a simplified formulation to evaluate the characteristic value of a population of samples ("design from samples", Annex D of EC0). Considering a Log-normal distribution, the formulation is the following:

$$X_k = exp(m_y - k_n \cdot s_y) \quad (1)$$

where m_y and s_y are respectively the estimations of mean value and standard deviation taken from the Log-normal distribution of samples, while k_n is a calibrated coefficient which takes into account the numbers of samples in the population and the type of distribution considered. For

Table 6
Results of distribution of Young's modulus for WAAM 308LSi stainless steel.

		Fractiles from statistical distribution				
		$E_{0.1\%}$	$E_{5\%}$	$E_{50\%}$	$E_{95\%}$	$E_{99.9\%}$
Young's modulus [MPa]	T	97	101	106	112	116
	L	106	117	132	148	163
	D	154	190	244	314	388

Table 5
Results of calibration for the design values of WAAM 308LSi stainless steel.

		5% and 0.1% fractiles from statistical distribution			Characteristic value, design value and safety factors according to EC0 [36]			EC3 recommendations for partial safety factors [35]
		$f_{y,5\%}$	$f_{y,0.1\%}$	$f_{y,5\%}/f_{y,0.1\%}$	f_{yk}	f_{yd}	γ_{m1}	γ_{M1}
0.2% proof stress [MPa]	T	321	296	1.08	310	301	1.03	1.10
	L	305	279	1.09	297	283	1.05	
	D	353	309	1.14	343	309	1.11	
		$f_{t,5\%}$	$f_{t,0.1\%}$	$f_{t,5\%}/f_{t,0.1\%}$	f_{tk}	f_{td}	γ_{m2}	γ_{M2}
Ultimate tensile strength [MPa]	T	469	408	1.15	443	424	1.05	1.25
	L	533	508	1.05	532	517	1.03	
	D	509	441	1.16	494	443	1.12	

a Log-normal distribution, the values of coefficient k_n as suggested by [36] are equal to: 2.18 for specimens T (6 samples,), 2.00 for specimens L (8 samples) and 1.89 for specimens D (12 samples).

Annex C of EC0 [36] provides also the formulation to compute the design value of the material property considered, based on the type of distribution and the probability of failure chosen for the design purposes. In the present case, the evaluations were performed considering a probability of non-exceedence of 10^{-3}, typically assumed when dealing with ultimate limit states, and corresponding to a target reliability index β equal to 3.8.

Therefore, the design value can be evaluated with the following expression:

$$X_d = \mu_X \cdot exp(-\alpha_R \cdot \beta \cdot V_X) \quad (2)$$

Where μ_X and V_X are the mean and coefficient of variation of the distribution considered, and α_R is the FORM sensitivity factor, usually taken equal to 0.8 for design resistances.

Thus, the partial safety factor of the considered material property can be estimated as the ratio between the computed characteristic and design values as follows:

$$\gamma_m = \frac{X_k}{X_d} \quad (3)$$

5.3. Comparison of the results from calibration

Table 5 provides an overview of the results of calibration according to Eurocode 0 [36], compared with the values of fractiles as evaluated from statistical distribution of the experimental results, as from Section 4.

In general, the results indicate a good correspondence between the values of 5% and 0.1% fractiles from the statistical distributions and the characteristic and design values as obtained according to Eurocode 0. In detail, the characteristic values calibrated according to Eurocode 0 are overall lower than the actual 5% fractile of the best-fit Log-normal distribution. This is due to the fact that for small sample sizes, the use of large values of k_n coefficient results in a characteristic value that corresponds to a fractile smaller than the 5% one. Consequently, in this case the characteristic values get closer to the design values and therefore the corresponding partial safety factors tend to reduce.

The anisotropic behavior with respect to the specimens orientation is also evidenced by the calibrated characteristic and design values and corresponding partial factors. In particular, as expected, the values of the partial safety factors (both for yielding and ultimate stress) for direction D tend to be larger. In any case, the values of partial safety factors suggested by EC3 [35] are in general, excluding the yielding stress along direction D, larger than those obtained in this study.

6. Considerations upon Young's modulus

Specific considerations on Young's modulus values are necessary to account for both the large anisotropy along the different orientations and for the intrinsic variability of the parameter. Indeed, standard Young's modulus values of stainless steel material exhibit a quite reduced variability that is commonly neglected in the design phase.

For this aim, specific fractiles (namely 0.1%, 5%, 50%, 95% and 99.9% fractiles) have been evaluated from the best-fit statistical distributions considering the three orientations. The values reported in Table 6 clearly evidence the anisotropic behavior of Young's modulus with respect to the different orientations of the specimen and intrinsic variability which therefore should be taken into account during the design phase.

7. Conclusions

This paper presents a first attempt to obtain design values for the main mechanical properties of 308LSi stainless steel specimens fabricated by Wire-and-Arc Additive Manufacturing (WAAM) process. The calibration accounts for the anisotropic behavior evidenced by the results of tensile tests carried out on samples oriented along the three directions with respect to the printing layers: along the deposition layer (longitudinal direction L), perpendicular to it (transversal direction T) and inclined 45° with respect to the deposition layer (diagonal direction D).

In detail, average values of 0.2% proof stress and ultimate tensile strength are consistent with the values commonly adopted for traditionally manufactured stainless steel (e.g. 350 MPa for 0.2% proof stress and 500 MPa for ultimate tensile strength), along the three main orientations tested. Young's modulus values present high variability based on the orientation of the specimens: for specimens cut along directions L and T, the Young's modulus values are on average 40% less than the common value adopted for traditionally-manufactured stainless steel members (200 GPa), while for specimens along direction D the average value is 20% higher than the reference one. This anisotropic behavior depends on the orientation of the microstructural grain growth perpendicular to the deposition layers. It induces an orthotropic elastic behavior along the two main directions (L and T), which results in higher values of elastic modulus at around 45°.

A first calibration of the design values and partial safety factors of both yielding and ultimate tensile stresses was carried out following two approaches. The first approach is based on the best-fit Log-normal distribution, while the second one is based on the experimental mean and standard deviation through the procedure explained in Annex D of EC0 [36]. For the first approach, the statistical analysis of the results of tensile tests allowed to obtain the distributions of 0.2% proof stress, ultimate tensile strength and Young's modulus. From the best-fit distributions, selected percentiles representative of design values have been evaluated.

The results from the two approaches show a good agreement between the values of the 5% and 0.1% percentiles of the statistical distributions and the corresponding characteristic and design values calibrated using the EC0 procedure. In particular, the characteristic values of 0.2% proof stress are between 300 and 350 MPa and the design ones between 280 and 310 MPa, varying depending on the orientation with respect to the deposition layer. The characteristic values of ultimate tensile strength are between 470 and 530 MPa and the design ones between 440 and 510 MPa, varying depending on the orientation with respect to the deposition layer. For both material properties, the corresponding partial safety factors vary from 1.03 to 1.12. The results from both approaches are in good agreement with the values suggested for stainless steel structures as in EC3 [35].

Additional considerations were made for the Young's modulus, for which specific fractiles (namely 0.1%, 5%, 50%, 95% and 99.9%) have been evaluated from best-fit Log-normal distributions considering the three main orientations of the specimens. Specific fractiles may be used depending upon different design considerations, either as lower or upper bounds.

The results presented in this work are intended as a first reference for structural engineers and producers dealing with the design of structures realized with WAAM members. The long term objective is to provide a contribution to deliver guidelines for the structural design of structures realized with WAAM-produced steel members.

CRediT authorship contribution statement

Vittoria Laghi: Conceptualization, Investigation, Writing - original draft. **Michele Palermo:** Conceptualization, Visualization, Writing - review & editing. **Giada Gasparini:** Writing - review & editing. **Milan Veljkovic:** Resources, Writing - review & editing. **Tomaso Trombetti:** Conceptualization, Supervision.

Declaration of Competing Interest

None.

Acknowledgements

The support of Dutch company MX3D held in Amsterdam is gratefully acknowledged for giving the additive-manufactured specimens tested.

Appendix A. Supplementary material

Supplementary data to this article can be found online at https://doi.org/10.1016/j.engstruct.2020.111314.

References

[1] Attaran M. The rise of 3-D printing: The advantages of additive manufacturing over traditional manufacturing. Bus Horiz 2017. https://doi.org/10.1016/j.bushor.2017.05.011.
[2] Thomas CL, Gaffney TM, Kaza S, Lee CH. Rapid prototyping of large scale aerospace structures. In: 1996 IEEE Aerosp Appl Conf; 1998, p. 219–30.
[3] Song Y, Yan Y, Zhang R, Xu D, Wang F. Manufacture of the die of an automobile deck part based on rapid prototyping and rapid tooling technology. J Mater Process Technol 2002. https://doi.org/10.1016/S0924-0136(01)01165-7.
[4] Giannatsis J, Dedoussis V. Additive fabrication technologies applied to medicine and health care: A review. Int J Adv Manuf Technol 2009;40:116–27. https://doi.org/10.1007/s00170-007-1308-1.
[5] Buchanan C, Gardner L. Metal 3D printing in construction: A review of methods, research, applications, opportunities and challenges. Eng Struct 2019;180:332–48. https://doi.org/10.1016/j.engstruct.2018.11.045.
[6] Galjaard S, Hofman S, Ren S. New Opportunities to Optimize Structural Designs in Metal by Using Additive Manufacturing. In: Block P, Knippers J, Mitra NJ, Wang W, editors. Adv. Archit. Geom. 2014, Cham: Springer International Publishing; 2015, p. 79–93.
[7] Raspall F, Banon C, Tay JC. AIRTABLE. Stainless steel printing for functional space frames. Comput Archit Des Res. Asia 2019;2019(1):113–22.
[8] Buchanan C, Matilainen VP, Salminen A, Gardner L. Structural performance of additive manufactured metallic material and cross-sections. J Constr Steel Res 2017;136:35–48. https://doi.org/10.1016/j.jcsr.2017.05.002.
[9] MX3D Webpage; n.d. www.mx3d.com.
[10] Dinovitzer M, Chen X, Laliberte J, Huang X, Frei H. Effect of wire and arc additive manufacturing (WAAM) process parameters on bead geometry and microstructure. Addit Manuf 2019;26:138–46. https://doi.org/10.1016/j.addma.2018.12.013.
[11] Skiba T, Baufeld B, Van Der Biest O. Microstructure and mechanical properties of stainless steel component manufactured by shaped metal deposition. ISIJ Int 2009;49:1588–91. https://doi.org/10.2355/isijinternational.49.1588.
[12] Niendorf T, Leuders S, Riemer A, Richard HA, Tröster T, Schwarze D. Highly anisotropic steel processed by selective laser melting. Metall Mater Trans B Process Metall Mater Process Sci 2013;44:794–6. https://doi.org/10.1007/s11663-013-9875-z.
[13] Guan K, Wang Z, Gao M, Li X, Zeng X. Effects of processing parameters on tensile properties of selective laser melted 304 stainless steel. Mater Des 2013;50:581–6. https://doi.org/10.1016/j.matdes.2013.03.056.
[14] Song B, Zhao X, Li S, Han C, Wei Q, Wen S, et al. Differences in microstructure and properties between selective laser melting and traditional manufacturing for fabrication of metal parts: A review. Front Mech Eng 2015;10:111–25. https://doi.org/10.1007/s11465-015-0341-2.
[15] Marinelli G, Martina F, Ganguly S, Williams S, Lewtas H, Hancock D, et al. Microstructure and thermal properties of unalloyed tungsten deposited by Wire + Arc Additive Manufacture. J Nucl Mater 2019. https://doi.org/10.1016/j.jnucmat.2019.04.049.
[16] Wu W, Xue J, Wang L, Zhang Z, Hu Y, Dong C. Forming process, microstructure, and mechanical properties of thin-walled 316L stainless steel using speed-cold-welding additive manufacturing. Metals (Basel) 2019;9.. https://doi.org/10.3390/met9010109.
[17] Posch G, Chladil K, Chladil H. Material properties of CMT—metal additive manufactured duplex stainless steel blade-like geometries. Weld World 2017;61:873–82. https://doi.org/10.1007/s40194-017-0474-5.
[18] Gu J, Wang X, Bai J, Ding J, Williams S, Zhai Y, et al. Deformation microstructures and strengthening mechanisms for the wire+arc additively manufactured Al-Mg4.5Mn alloy with inter-layer rolling. Mater Sci Eng A 2018;712:292–301.. https://doi.org/10.1016/j.msea.2017.11.113.
[19] Derekar KS. A review of wire arc additive manufacturing and advances in wire arc additive manufacturing of aluminium. Mater Sci Technol (United Kingdom) 2018;34:895–916. https://doi.org/10.1080/02670836.2018.1455012.
[20] Haden CV, Zeng G, Carter FM, Ruhl C, Krick BA, Harlow DG. Wire and arc additive manufactured steel: Tensile and wear properties. Addit Manuf 2017;16:115–23. https://doi.org/10.1016/j.addma.2017.05.010.
[21] Gordon JV, Haden CV, Nied HF, Vinci RP, Harlow DG. Fatigue crack growth anisotropy, texture and residual stress in austenitic steel made by wire and arc additive manufacturing. Mater Sci Eng A 2018;724:431–8. https://doi.org/10.1016/j.msea.2018.03.075.
[22] Kyvelou P, Slack H, Mountanou DD, Wadee MA, Britton T Ben, Buchanan C, et al. Mechanical and microstructural testing of wire and arc additively manufactured sheet material. Mater Des 2020:108675. https://doi.org/10.1016/J.MATDES.2020.108675.
[23] Laghi V, Palermo M, Gasparini G, Girelli VA, Trombetti T. Geometrical characterization of Wire-and-Arc Additive Manufactured steel elements. VBRI Press Adv Mater Lett 2019;10:695–9.
[24] Laghi V, Palermo M, Gasparini G, Girelli VA, Trombetti T. Experimental results for structural design of Wire-and-Arc Additive Manufactured stainless steel members. J Constr Steel Res 2019.
[25] Laghi V, Palermo M, Tonelli L, Gasparini G, Ceschini L, Trombetti T. Tensile properties and microstructural features of 304L austenitic stainless steel produced by wire-and-arc additive manufacturing. Int J Adv Manuf Technol 2020:3693–705. https://doi.org/10.1007/s00170-019-04868-8.
[26] Wong KV, Hernandez A. A Review of Additive Manufacturing. ISRN Mech Eng 2012;2012:1–10. https://doi.org/10.5402/2012/208760.
[27] Williams SW, Martina F, Addison AC, Ding J, Pardal G, Colegrove P. Wire + Arc additive manufacturing. Mater Sci Technol (United Kingdom) 2016;32:641–7. https://doi.org/10.1179/1743284715Y.0000000073.
[28] Uziel A. Looking at large-scale, arc-based Additive Manufacturing. Weld J 2016;4..
[29] Ji L, Lu J, Liu C, Jing C, Fan H, Ma S. Microstructure and mechanical properties of 304L steel fabricated by arc additive manufacturing. MATEC Web Conf 2017;128. https://doi.org/10.1051/matecconf/201712803006.
[30] Kim IS, Son KJ, Yang YS, Yaragada PKDV. Sensitivity analysis for process parameters in GMA welding processes using a factorial design method. Int J Mach Tools Manuf 2003;43:763–9. https://doi.org/10.1016/S0890-6955(03)00054-3.
[31] Yilmaz O, Ugla AA. Microstructure characterization of SS308LSi components manufactured by GTAW-based additive manufacturing: shaped metal deposition using pulsed current arc. Int J Adv Manuf Technol 2017;89:13–25. https://doi.org/10.1007/s00170-016-9053-y.
[32] Joosten SK. Printing a stainless steel bridge: an exploration of structural properties of stainless steel additive manufactured for civil engineering purposes. University of Technology Delft; 2015.
[33] Van Bolderen GS. Exploration of stability of 3D-printed steel members. University of Technology Delft 2017.
[34] Metallic materials — Tensile testing — Part 1: Method of test at room temperature Matériaux métalliques — Essai de traction — Partie 1: Méthode d'essai à température ambiante. Iso 6892-1; 2009.
[35] European Committee for Standardization (CEN). EN 1993 1-4: Eurocode 3 - Design of steel structures, part 1-4: General rules, supplementary rules for stainless steel; 2015.
[36] European Committee for Standardization (CEN). EN 1990: Eurocode 0 - Basis of Structural Design; 2002.
[37] Ballio G, Mazzolani FM. Strutture in acciaio. Arnoldo Mondadori Editore 1979.
[38] Jr FJM. The Kolmogorov-Smirnov Test for Goodness of Fit. J Am Stat Assoc 1951;46:68–78. https://doi.org/10.1080/01621459.1951.10500769.